Measurements of transverse energy distributions in Au+Au collisions at $\sqrt{s_{NN}}$=200 GeV

J. Adams,[3] M. M. Aggarwal,[29] Z. Ahammed,[43] J. Amonett,[20] B. D. Anderson,[20] D. Arkhipkin,[13] G. S. Averichev,[12] Y. Bai,[27] J. Balewski,[17] O. Barannikova,[32] L. S. Barnby,[3] J. Baudot,[18] S. Bekele,[28] V. V. Belaga,[12] R. Bellwied,[46] J. Berger,[14] B. I. Bezverkhny,[48] S. Bharadwaj,[33] V. S. Bhatia,[29] H. Bichsel,[45] A. Billmeier,[46] L. C. Bland,[4] C. O. Blyth,[3] B. E. Bonner,[34] M. Botje,[27] A. Boucham,[38] A. Brandin,[25] A. Bravar,[4] M. Bystersky,[11] R. V. Cadman,[1] X. Z. Cai,[37] H. Caines,[48] M. Calderón de la Barca Sánchez,[4] J. Carroll,[21] J. Castillo,[21] D. Cebra,[7] Z. Chajecki,[44] P. Chaloupka,[11] S. Chattopdhyay,[43] H. F. Chen,[36] Y. Chen,[8] J. Cheng,[41] M. Cherney,[10] A. Chikanian,[48] W. Christie,[4] J. P. Coffin,[18] T. M. Cormier,[46] J. G. Cramer,[45] H. J. Crawford,[6] D. Das,[43] S. Das,[43] M. M. de Moura,[35] A. A. Derevschikov,[31] L. Didenko,[4] T. Dietel,[14] W. J. Dong,[8] X. Dong,[36] J. E. Draper,[7] F. Du,[48] A. K. Dubey,[15] V. B. Dunin,[12] J. C. Dunlop,[4] M. R. Dutta Mazumdar,[43] V. Eckardt,[23] W. R. Edwards,[21] L. G. Efimov,[12] V. Emelianov,[25] J. Engelage,[6] G. Eppley,[34] B. Erazmus,[38] M. Estienne,[38] P. Fachini,[4] J. Faivre,[18] R. Fatemi,[17] J. Fedorisin,[12] K. Filimonov,[21] P. Filip,[11] E. Finch,[48] V. Fine,[4] Y. Fisyak,[4] K. J. Foley,[4] K. Fomenko,[12] J. Fu,[41] C. A. Gagliardi,[39] J. Gans,[48] M. S. Ganti,[43] L. Gaudichet,[38] F. Geurts,[34] V. Ghazikhanian,[8] P. Ghosh,[43] J. E. Gonzalez,[8] O. Grachov,[46] O. Grebenyuk,[27] D. Grosnick,[42] S. M. Guertin,[8] Y. Guo,[46] A. Gupta,[19] T. D. Gutierrez,[7] T. J. Hallman,[4] A. Hamed,[46] D. Hardtke,[21] J. W. Harris,[48] M. Heinz,[2] T. W. Henry,[39] S. Hepplemann,[30] B. Hippolyte,[48] A. Hirsch,[32] E. Hjort,[21] G. W. Hoffmann,[40] H. Z. Huang,[8] S. L. Huang,[36] E. W. Hughes,[5] T. J. Humanic,[28] G. Igo,[8] A. Ishihara,[40] P. Jacobs,[21] W. W. Jacobs,[17] M. Janik,[44] H. Jiang,[8] P. G. Jones,[3] E. G. Judd,[6] S. Kabana,[2] K. Kang,[41] M. Kaplan,[9] D. Keane,[20] V. Yu. Khodyrev,[31] J. Kiryluk,[22] A. Kisiel,[44] E. M. Kislov,[12] J. Klay,[21] S. R. Klein,[21] A. Klyachko,[17] D. D. Koetke,[42] T. Kollegger,[14] M. Kopytine,[20] L. Kotchenda,[25] M. Kramer,[26] P. Kravtsov,[25] V. I. Kravtsov,[31] K. Krueger,[1] C. Kuhn,[18] A. I. Kulikov,[12] A. Kumar,[29] C. L. Kunz,[9] R. Kh. Kutuev,[13] A. A. Kuznetsov,[12] M. A. C. Lamont,[48] J. M. Landgraf,[4] S. Lange,[14] F. Laue,[4] J. Lauret,[4] A. Lebedev,[4] R. Lednicky,[12] S. Lehocka,[12] M. J. LeVine,[4] C. Li,[36] Q. Li,[46] Y. Li,[41] S. J. Lindenbaum,[26] M. A. Lisa,[28] F. Liu,[47] L. Liu,[47] Q. J. Liu,[45] Z. Liu,[47] T. Ljubicic,[4] W. J. Llope,[34] H. Long,[8] R. S. Longacre,[4] M. Lopez-Noriega,[28] W. A. Love,[4] Y. Lu,[47] T. Ludlam,[4] D. Lynn,[4] G. L. Ma,[37] J. G. Ma,[8] Y. G. Ma,[37] D. Magestro,[28] S. Mahajan,[19] D. P. Mahapatra,[15] R. Majka,[48] L. K. Mangotra,[19] R. Manweiler,[42] S. Margetis,[20] C. Markert,[48] L. Martin,[38] J. N. Marx,[21] H. S. Matis,[21] Yu. A. Matulenko,[31] C. J. McClain,[1] T. S. McShane,[10] F. Meissner,[21] Yu. Melnick,[31] A. Meschanin,[31] M. L. Miller,[22] Z. Milosevich,[9] N. G. Minaev,[31] C. Mironov,[20] A. Mischke,[27] D. Mishra,[15] J. Mitchell,[34] B. Mohanty,[43] L. Molnar,[32] C. F. Moore,[40] M. J. Mora-Corral,[23] D. A. Morozov,[31] V. Morozov,[21] M. G. Munhoz,[35] B. K. Nandi,[43] T. K. Nayak,[43] J. M. Nelson,[3] P. K. Netrakanti,[43] V. A. Nikitin,[13] L. V. Nogach,[31] B. Norman,[20] S. B. Nurushev,[31] G. Odyniec,[21] A. Ogawa,[4] V. Okorokov,[25] M. Oldenburg,[21] D. Olson,[21] S. K. Pal,[43] Y. Panebratsev,[12] S. Y. Panitkin,[4] A. I. Pavlinov,[46] T. Pawlak,[44] T. Peitzmann,[27] V. Perevoztchikov,[4] C. Perkins,[6] W. Peryt,[44] V. A. Petrov,[13] S. C. Phatak,[15] R. Picha,[7] M. Planinic,[49] J. Pluta,[44] N. Porile,[32] J. Porter,[45] A. M. Poskanzer,[21] M. Potekhin,[4] E. Potrebenikova,[12] B. V. K. S. Potukuchi,[19] D. Prindle,[45] C. Pruneau,[46] J. Putschke,[23] G. Rai,[21] G. Rakness,[30] R. Raniwala,[33] S. Raniwala,[33] O. Ravel,[38] R. L. Ray,[40] S. V. Razin,[12] D. Reichhold,[32] J. G. Reid,[45] G. Renault,[38] F. Retiere,[21] A. Ridiger,[25] H. G. Ritter,[21] J. B. Roberts,[34] O. V. Rogachevskiy,[12] J. L. Romero,[7] A. Rose,[46] C. Roy,[38] L. Ruan,[36] I. Sakrejda,[21] S. Salur,[48] J. Sandweiss,[48] I. Savin,[13] P. S. Sazhin,[12] J. Schambach,[40] R. P. Scharenberg,[32] N. Schmitz,[23] L. S. Schroeder,[21] K. Schweda,[21] J. Seger,[10] P. Seyboth,[23] E. Shahaliev,[12] M. Shao,[36] W. Shao,[5] M. Sharma,[29] W. Q. Shen,[37] K. E. Shestermanov,[31] S. S. Shimanskiy,[12] F. Simon,[23] R. N. Singaraju,[43] G. Skoro,[12] N. Smirnov,[48] R. Snellings,[27] G. Sood,[42] P. Sorensen,[21] J. Sowinski,[17] J. Speltz,[18] H. M. Spinka,[1] B. Srivastava,[32] A. Stadnik,[12] T. D. S. Stanislaus,[42] R. Stock,[14] A. Stolpovsky,[46] M. Strikhanov,[25] B. Stringfellow,[32] A. A. P. Suaide,[35] E. Sugarbaker,[28] C. Suire,[4] M. Sumbera,[11] B. Surrow,[22] T. J. M. Symons,[21] A. Szanto de Toledo,[35] P. Szarwas,[44] A. Tai,[8] J. Takahashi,[35] A. H. Tang,[27] T. Tarnowsky,[32] D. Thein,[8] J. H. Thomas,[21] S. Timoshenko,[25] M. Tokarev,[12] T. A. Trainor,[45] S. Trentalange,[8] R. E. Tribble,[39] O. Tsai,[8] J. Ulery,[32] T. Ullrich,[4] D. G. Underwood,[1] A. Urkinbaev,[12] G. Van Buren,[4] M. van Leeuwen,[21] A. M. Vander Molen,[24] R. Varma,[16] I. M. Vasilevski,[13] A. N. Vasiliev,[31] R. Vernet,[18] S. E. Vigdor,[17] V. P. Viyogi,[43] S. Vokal,[12] S. A. Voloshin,[46] M. Vznuzdaev,[25] B. Waggoner,[10] F. Wang,[32] G. Wang,[20] G. Wang,[5] X. L. Wang,[36] Y. Wang,[40] Y. Wang,[41] Z. M. Wang,[36] H. Ward,[40] J. W. Watson,[20] J. C. Webb,[17] R. Wells,[28] G. D. Westfall,[24] A. Wetzler,[21] C. Whitten, Jr.,[8] H. Wieman,[21] S. W. Wissink,[17] R. Witt,[2] J. Wood,[8] J. Wu,[36] N. Xu,[21] Z. Xu,[4] Z. Z. Xu,[36] E. Yamamoto,[21] P. Yepes,[34] V. I. Yurevich,[12] Y. V. Zanevsky,[12] H. Zhang,[4] W. M. Zhang,[20] Z. P. Zhang,[36] P. A. Zolnierczuk,[17] R. Zoulkarneev,[13] Y. Zoulkarneeva,[13] and A. N. Zubarev[12]

(STAR Collaboration)

[1]*Argonne National Laboratory, Argonne, Illinois 60439, USA*
[2]*University of Bern, Bern, Switzerland CH-3012*
[3]*University of Birmingham, Birmingham, United Kingdom*
[4]*Brookhaven National Laboratory, Upton, New York 11973, USA*
[5]*California Institute of Technology, Pasadena, California 91125, USA*
[6]*University of California, Berkeley, California 94720, USA*
[7]*University of California, Davis, California 95616, USA*
[8]*University of California, Los Angeles, California 90095, USA*
[9]*Carnegie Mellon University, Pittsburgh, Pennsylvania 15213, USA*
[10]*Creighton University, Omaha, Nebraska 68178, USA*

[11]*Nuclear Physics Institute AS CR, 250 68 Řež/Prague, Czech Republic*
[12]*Laboratory for High Energy (JINR), Dubna, Russia*
[13]*Particle Physics Laboratory (JINR), Dubna, Russia*
[14]*University of Frankfurt, Frankfurt, Germany*
[15]*Insitute of Physics, Bhubaneswar 751005, India*
[16]*Indian Institute of Technology, Mumbai, India*
[17]*Indiana University, Bloomington, Indiana 47408, USA*
[18]*Institut de Recherches Subatomiques, Strasbourg, France*
[19]*University of Jammu, Jammu 180001, India*
[20]*Kent State University, Kent, Ohio 44242, USA*
[21]*Lawrence Berkeley National Laboratory, Berkeley, California 94720, USA*
[22]*Massachusetts Institute of Technology, Cambridge, Massachusetts 02139-4307, USA*
[23]*Max-Planck-Institut für Physik, Munich, Germany*
[24]*Michigan State University, East Lansing, Michigan 48824, USA*
[25]*Moscow Engineering Physics Institute, Moscow Russia*
[26]*City College of New York, New York City, New York 10031, USA*
[27]*NIKHEF, Amsterdam, The Netherlands*
[28]*Ohio State University, Columbus, Ohio 43210, USA*
[29]*Panjab University, Chandigarh 160014, India*
[30]*Pennsylvania State University, University Park, Pennsylvania 16802, USA*
[31]*Institute of High Energy Physics, Protvino, Russia*
[32]*Purdue University, West Lafayette, Indiana 47907, USA*
[33]*University of Rajasthan, Jaipur 302004, India*
[34]*Rice University, Houston, Texas 77251, USA*
[35]*Universidade de Sao Paulo, Sao Paulo, Brazil*
[36]*University of Science & Technology of China, Anhui 230027, China*
[37]*Shanghai Institute of Applied Physics, Shanghai 201800, People's Republic of China*
[38]*SUBATECH, Nantes, France*
[39]*Texas A&M University, College Station, Texas 77843, USA*
[40]*University of Texas, Austin, Texas 78712, USA*
[41]*Tsinghua University, Beijing, People's Republic of China*
[42]*Valparaiso University, Valparaiso, Indiana 46383, USA*
[43]*Variable Energy Cyclotron Centre, Kolkata 700064, India*
[44]*Warsaw University of Technology, Warsaw, Poland*
[45]*University of Washington, Seattle, Washington 98195, USA*
[46]*Wayne State University, Detroit, Michigan 48201, USA*
[47]*Institute of Particle Physics, CCNU (HZNU), Wuhan 430079, China*
[48]*Yale University, New Haven, Connecticut 06520, USA*
[49]*University of Zagreb, Zagreb HR-10002, Croatia*
(Received 2 July 2004; published 23 November 2004)

Transverse energy (E_T) distributions have been measured for Au+Au collisions at $\sqrt{s_{NN}}=200$ GeV by the STAR Collaboration at RHIC. E_T is constructed from its hadronic and electromagnetic components, which have been measured separately. E_T production for the most central collisions is well described by several theoretical models whose common feature is large energy density achieved early in the fireball evolution. The magnitude and centrality dependence of E_T per charged particle agrees well with measurements at lower collision energy, indicating that the growth in E_T for larger collision energy results from the growth in particle production. The electromagnetic fraction of the total E_T is consistent with a final state dominated by mesons and independent of centrality.

DOI: 10.1103/PhysRevC.70.054907 PACS number(s): 25.75.Dw

I. INTRODUCTION

High energy nuclear collisions at the Relativistic Heavy Ion Collider (RHIC) [1] have opened a new domain in the exploration of strongly interacting matter at very high energy density. High temperatures and densities may be generated in the most central (head-on) nuclear collisions, perhaps creating the conditions in which a phase of deconfined quarks and gluons exists [2,3]. The fireball produced in such collisions undergoes a complex dynamical evolution, and understanding of the conditions at the hot, dense early phase of the collision requires understanding of the full reaction dynamics.

Transverse energy E_T is generated by the initial scattering of the partonic constituents of the incoming nuclei and possibly also by reinteractions among the produced partons and hadrons [4,5]. If the fireball of produced quanta breaks apart quickly without significant reinteraction, the observed transverse energy per unit rapidity dE_T/dy will be the same as that generated by the initial scatterings. At the other extreme, if the system reinteracts strongly, achieving local equilibrium early and maintaining it throughout the expansion, dE_T/dy will decrease significantly during the fireball evolution due to the longitudinal work performed by the hydrodynamic pressure [6,7]. This decrease will, however, be moderated by the buildup of transverse hydrodynamic flow, which increases E_T [8]. Finally, gluon saturation in the wave function of the colliding heavy nuclei can delay the onset of hydrodynamic flow, reducing the effective pressure and thereby also reducing the difference between initially generated and observed E_T [9].

E_T production in nuclear collisions has been studied at lower $\sqrt{s}$ at the AGS and CERN [10–14] and at RHIC [15]. Within the framework of boost-invariant hydrodynamics [16], these measurements suggest that energy densities have been achieved at the SPS [13] that exceed the deconfinement energy density predicted by lattice QCD [17]. However, from the foregoing discussion it is seen that several competing dynamical effects can contribute to the observed dE_T/dy. While the measurement of E_T alone cannot disentangle these effects, a systematic study of E_T together with other global event properties, in particular charged multiplicity and mean transverse momentum $\langle p_T \rangle$, may impose significant constraints on the collision dynamics [8].

In this paper, we report the measurement of E_T distributions from Au+Au collisions at $\sqrt{s_{NN}}=200$ GeV per nucleon-nucleon pair, measured by the STAR detector at RHIC. E_T is measured using a patch of the STAR Electromagentic Calorimeter, with acceptance $0<\eta<1$ and $\Delta\phi=60°$, together with the STAR Time Projection Chamber. E_T is separated into its hadronic and electromagnetic components, with the latter dominated by π^0 and η decays. The centrality dependence of E_T and E_T per charged particle is studied, and comparisons are made to models and to measurements at lower energy.

A high-temperature deconfined phase could be a significant source of low to intermediate p_T photons [18]. An excess of photons above those expected from hadronic decays has been observed at the SPS for $p_T>1.5$ GeV/c [19]. We investigate this effect through the study of the electromagnetic component of E_T.

Section II describes the experimental setup used for the analysis. Section III presents the analysis of the hadronic component of the transverse energy. In Sec. IV, the analysis of the electromagnetic transverse energy is presented. In Sec. V, we discuss the scaling of E_T with the energy of the colliding system and the number of participants $N_{\rm part}$ and binary collisions $N_{\rm bin}$ [20], together with theoretical expectations for this scaling. We also discuss the behavior of the electromagnetic component of the transverse energy with the collision energy and centrality. Section VI is a summary and discussion of the main results.

II. STAR EXPERIMENT

This analysis is based on 150 K minimum bias Au+Au collisions measured by the STAR detector in the 2001 RHIC run. STAR [21] is a large acceptance, multipurpose experiment comprising several detector systems inside a large solenoidal magnet. In the following, we describe the detectors which are relevant to the present analysis.

The barrel electromagnetic calorimeter (EMC) [22] is a lead-scintillator sampling electromagnetic calorimeter with equal volumes of lead and scintillator. It has a radius of 2.3 m and is situated just inside the coils of the STAR solenoidal magnet. The electromagnetic energy resolution of the detector is $\delta E/E \sim 16\%/\sqrt{E\ (\mathrm{GeV})}$. The results presented in this work used the first EMC patch installed for the 2001 RHIC run consisting of 12 modules, ~10% of the full planned detector, with coverage $0<\eta<1$ and $\Delta\phi=60°$. Each EMC module is composed of 40 towers (20 towers in η by 2 towers in ϕ) constructed to project to the center of the STAR detector. The transverse dimensions of a tower are approximately 10×10 cm^2, which at the radius of the front face of the detector correspond to a phase space interval of $(\Delta\eta,\Delta\phi)=(0.05,0.05)$. The tower depth is 21 radiation lengths (X_0), corresponding to approximately one hadronic interaction length. When fully installed, the complete barrel will consist of 120 modules with pseudorapidity coverage $-1<\eta<1$ and full azimuthal coverage.

The time projection chamber (TPC) [23] has a pseudorapidity coverage of $|\eta|<1.2$ for collisions in the center of STAR, with full azimuthal coverage. In this work, the acceptance of the measurement was limited by the acceptance of the EMC. For charged tracks in the acceptance, the TPC provides up to 45 independent spatial and specific ionization dE/dx measurements. The dE/dx measurement in combination with the momentum measurement determines the particle mass within limited kinematic regions.

The magnetic field was 0.5 T. TPC track quality cuts included z-coordinate (longitudinal axis) selection of the collision vertex within 20 cm of the TPC center and a minimum TPC track space point cut of 10. Typical TPC momentum resolution for the data in this work is characterized by $\delta k/k \sim 0.0078+0.0098\cdot p_T\ (\mathrm{GeV}/c)$ [23] in which k is the track curvature, proportional to $1/p_T$. Typical resolution of dE/dx measurement is ~8%. Additional discussion of TPC analysis is given in the following sections and a more detailed description of the TPC itself can be found in Ref. [23].

The event trigger consisted of the coincidence of signals from the two zero degree calorimeters (ZDC) [24], located at $\theta<2$ mrad about the beam downstream of the first accelerator dipole magnet and sensitive to spectator neutrons. These calorimeters provide a minimum bias trigger which, after collision vertex reconstruction, corresponds to $97\pm3\%$ of the geometric cross section $\sigma_{\rm geom}^{\rm Au+Au}$. The events were analyzed in centrality bins based on the charged particle multiplicity in $|\eta|<0.5$.

The procedures used in the analysis provide independent measurement of electromagnetic transverse energy and the transverse energy carried by charged hadrons. This latter quantity, corrected to take into account the contribution of

the long-lived neutral hadrons, is designated the hadronic transverse energy. The hadronic component of the transverse energy is obtained from momentum analyzed tracks in the TPC while the electromagnetic fraction is derived from the electromagnetic calorimeter data corrected for hadronic contamination using TPC tracking. In the following sections, we describe how each of these contributions was analyzed to obtain the total transverse energy E_T measurement.

III. HADRONIC TRANSVERSE ENERGY (E_T^{had})

The hadronic transverse energy E_T^{had} is defined as

$$E_T^{\mathrm{had}} = \sum_{\mathrm{hadrons}} E^{\mathrm{had}} \sin\theta, \tag{1}$$

where the sum runs over all hadrons produced in the collision, except π^0 and η. θ is the polar angle relative to the beam axis and the collision vertex position. E^{had} is defined for nucleons as kinetic energy, for antinucleons as kinetic energy plus twice the rest mass, and for all other particles as the total energy. E_T^{had} is measured using charged particle tracks in the TPC via

$$E_T^{\mathrm{had}} = C_0 \sum_{\mathrm{tracks}} C_1(ID,p) E_{\mathrm{track}}(ID,p) \sin\theta. \tag{2}$$

The sum includes all tracks from the primary vertex in the ranges $0<\eta<1$ and $\Delta\phi=60°$. C_0 is a correction factor defined as

$$C_0 = \frac{1}{f_{\mathrm{acc}}} \frac{1}{f_{p_T\mathrm{cut}}} \frac{1}{f_{\mathrm{neutral}}} \tag{3}$$

that includes the effective acceptance $f_{\mathrm{acc}}=\Delta\phi/2\pi$, the correction f_{neutral}, for long-lived neutral hadrons not measured by the TPC, and $f_{p_T\mathrm{cut}}$, for the TPC low momentum cutoff. $E_{\mathrm{track}}(ID,p)$ is the energy associated with the particular track, either total or kinetic, as described above, computed from the measured momentum and particle identity (ID) as described below. The factor $C_1(ID,p)$ is defined as

$$C_1(ID,p) = f_{\mathrm{bg}}(p_T) \frac{1}{f_{\mathrm{notID}}} \frac{1}{\mathrm{eff}(p_T)}, \tag{4}$$

which includes the corrections for the uncertainty in the particle ID determination, f_{notID}, momentum dependent tracking efficiency, $\mathrm{eff}(p_T)$, and momentum dependent backgrounds, $f_{\mathrm{bg}}(p_T)$. Next, we describe the corrections included in these two factors.

Particle identification was carried out using the measurements of momentum and truncated mean specific ionization $\langle dE/dx\rangle$ in the TPC. For $p_T<1$ GeV/c, assignment was made to the most probable particle type relative to the Bethe-Bloch expectation. Particles were assumed to be pions if $\langle dE/dx\rangle$ differed from this expectation by more than three standard deviations, or if $p_T>1$ GeV/c. The uncertainty in this procedure was gauged by calculating E_T^{had} for $p_T<1$ GeV/c both with the correct particle assignments and with all particles assumed to be pions. The ratio of these values for E_T^{had} is applied as a correction for particles that cannot be identified, yielding an overall correction factor to E_T^{had} of $f_{\mathrm{notID}}=0.96\pm0.02$. Because this correction was calculated from low momentum particles, it does not account for the centrality variations in the particle ratios with $p_T>1$ GeV/c [25]. On the other hand, particles at $p_T>1$ GeV/c account for about 20% of the total number of particles. Taking into account the centrality-dependence increases in the p/π and K/π ratios at higher p_T generates a change in the estimated hadronic E_T on the order of 2%, which is within the systematic error of f_{notID}.

Only tracks with a transverse momentum $p_T>0.15$ GeV/c were accepted because the tracking efficiency drops rapidly below this value. GEANT [26] detector simulations of HIJING [27] events demonstrate that this cut excludes 5% of the total E_T^{had}. A correction $f_{p_T\mathrm{cut}}$ for this effect is included in C_0. Taking all simulated tracks for $p_T>0.15$ GeV/c and calculating the energy assuming pions in two extreme cases, one with momentum $p=0$ and the other with $p=0.15$ GeV/c, resulted in a variation of 3% in E_T^{had}, which was assigned as the systematic uncertainty due to this correction.

Since only primary charged tracks measured by the TPC are used in this analysis, we need to correct E_T^{had} to include the contribution from long-lived neutral hadrons, principally $n(\overline{n}), K_L^0, K_S^0$, and $\Lambda(\overline{\Lambda})$. The correction factor applied to the data, defined as $f_{\mathrm{neutral}}=E_T^{\mathrm{charged}}/(E_T^{\mathrm{charged}}+E_T^{\mathrm{neutral}})$, can be estimated using measurements by STAR at 130 GeV [28–32]. We assume, based on HIJING simulations, that f_{neutral} does not change significantly from 130 GeV to 200 GeV. We assume that the spectrum shape and yield for K_L^0 are the same as for K_S^0. The same approximation was applied in the case of $n(\overline{n})$, after subtraction of the contribution from $\overline{\Lambda}$ decays from the measured $\overline{p}$ yield, and the measured STAR $\overline{p}/p$ ratio [28]. Using this procedure we obtained a value of $f_{\mathrm{neutral}}=0.81\pm0.02$. The uncertainty on this correction was estimated from the uncertainties in the measured STAR spectra. A cross check of these correction factors utilizing 200 GeV measurements [33] generates variations well within the assigned systematic uncertainties.

The correction $f_{\mathrm{bg}}(p_T)$ for background, consisting of electrons, weak decays and secondary tracks that are misidentified as primary, depends on the type of the track and is divided into two separate corrections. The first is for the electrons which are misidentified as hadrons. This correction was estimated using the shape of the electron spectrum obtained from HIJING and GEANT simulations and the absolute yield from STAR data in the region where electrons are identified with high purity using the TPC dE/dx measurements (essentially below 300 MeV). The second term is due to weak decays, which have been included in f_{neutral} and therefore must be excluded from the primary track population to avoid double counting of their energy. In this case, the correction factor was calculated by embedding simulated particles into real events. By comparison between the simulated particles and the reconstructed ones, the fraction of secondary tracks assigned as primary was evaluated. Λ and K^0 were simulated using the experimental yield and spectral shape measured by STAR [31,32].

The TPC reconstruction efficiency, $\mathrm{eff}(p_T)$, was also determined by embedding simulated tracks into real events and

TABLE I. Corrections and systematic uncertainties for hadronic energy $E_T^{\rm had}$ for the 5% most central collisions. The quadrature sum of all the systematic uncertainties results in a total of 6.1%. The upper part of the table shows the global corrections included in C_0 and the bottom part shows track-wise corrections included in $C_1(ID,p)$. In this case, the correction values for $p_T=0.25$ GeV/c and 1.0 GeV/c are shown.

Description	Correction
$f_{p_T\rm cut}$	0.95 ± 0.03
$f_{\rm neutral}$	0.81 ± 0.02
$f_{\rm notID}$	0.96 ± 0.02
$f_{\rm bg}(p_T)$	0.84 ± 0.02(0.25 GeV/c)
	0.94 ± 0.02(1.0 GeV/c)
eff(p_T)	0.70 ± 0.04(0.25 GeV/c)
	0.80 ± 0.04(1.0 GeV/c)

comparing the simulated input and the final reconstructed event. In order to evaluate the effect of different particle species in the reconstruction efficiency, pions, kaons, and protons were embedded in the real events. In this work, the charged track efficiency correction is the average, weighted by the relative populations of each of these species. The track reconstruction efficiency depends on the transverse momentum of the tracks and the total track density. For central events the efficiency is about 0.7 for tracks with $p_T=0.25$ GeV/c and reaches a plateau at about 0.8 for $p_T>0.4$ GeV/c. This efficiency correction includes the efficiency for track reconstruction, the probability for track splitting, ghost tracks, and dead regions of the TPC.

The resulting systematic uncertainties, taking into account all corrections, combine in quadrature to a systematic uncertainty estimate of 6.1% on $E_T^{\rm had}$. In Table I we summarize all individual corrections and the corresponding systematic uncertainties.

HIJING and GEANT simulations of $E_T^{\rm had}$ measured in the acceptance of this study generate event-wise fluctuations of about 10%. Simulations utilizing a substantially larger acceptance $(0<\eta<1, 0<\phi<2\pi)$ generate event-wise fluctuations of about 4%, with this latter resolution resulting mainly from tracking efficiency and neutral hadron corrections.

The final $E_T^{\rm had}$ distribution is corrected for vertex reconstruction efficiency. Peripheral events have lower vertex reconstruction efficiency which suppresses the transverse energy distributions with respect to more central events. The vertex reconstruction efficiency depends on the number of tracks measured in the TPC and varies from 70% to 97%.

IV. ELECTROMAGNETIC TRANSVERSE ENERGY ($E_T^{\rm em}$)

The electromagnetic transverse energy $E_T^{\rm em}$ is the sum of the measured transverse energy of electrons, positrons, and photons. The largest fraction of this energy comes from π^0 decays. Electrons (and positrons) are included because more than 90% of them are produced in the conversion of photons in detector materials. The energy of photons and electrons is fully measured by the calorimeter. There is also a contribution from charged and neutral hadrons produced in the collision that is significant and must be subtracted to permit a measurement of $E_T^{\rm em}$. In order to remove the hadronic contribution from the measurement, we studied the full spatial profiles of energy deposition by identified hadrons in the EMC. An extensive experimental library of hadronic shower clusters in the calorimeter has been obtained which, in conjunction with TPC tracking, allow a correction for the hadronic background in the calorimeter.

Section IV A discusses the calibration of the EMC using minimum ionizing particles and electrons, while Sec. IV B discusses the correction for hadronic energy deposition in the EMC and Sec. IV C discusses the determination of $E_T^{\rm em}$.

A. Calibration of EMC

Hadrons striking the EMC deposit a widely fluctuating fraction of their incident energy through hadronic showers. In addition, ~30–40 % of all high energy charged hadrons penetrate the entire depth of the EMC without hadronic interaction. If such a nonshowering primary charged hadron has sufficient momentum, it will behave like a minimum ionizing particle (MIP) as it transits each of the scintillator layers, resulting in uniform total energy deposition which will be nearly independent of the incident momentum but will vary linearly with the total thickness of the scintillator traversed. Due to the projective nature of the detector, the total length of the scintillator increases with increasing η. The MIP peak therefore varies from 250 MeV at small η to 350 MeV at large η. The absolute energy of the MIP peak and its η dependence was determined from cosmic rays and test beam measurements [34].

The use of MIP particles to calibrate the EMC *in situ* is convenient and provides a precision tool to track the calibration of the detector over time. In a procedure to minimize systematic uncertainties in the calibration, tracks with $p>1.25$ GeV/c in the TPC from relatively low multiplicity events are extrapolated to the EMC towers where they are required to be isolated from neighboring charged tracks in a 3×3 tower patch ($\Delta\eta\times\Delta\phi=0.15\times0.15$) which has a minimum size of ~30 cm $\times$ 30 cm ($\eta=0$). Figure 1 shows a typical MIP spectrum measured under these conditions using minimum bias Au+Au events. This example shows the pseudorapidity interval $0.2<\eta<0.3$. Similar spectra are observed in all η bins and provide an absolute calibration in the energy range less than ~2 GeV, with an estimated systematic uncertainty of ~5% [34].

An absolute calibration over a much wider energy range is obtained using identified electrons tracked with the TPC. This was done by selecting high momentum $(1.5<p<5.0$ GeV/$c)$ electrons reconstructed in the TPC. Electron candidates are selected by dE/dx measurement in the TPC. Although the purity of the electron candidates sample in this momentum range is poorer than for low momentum, the hadronic rejection factor obtained from the TPC dE/dx provides a clear electron signal in the calorimeter. Bethe-Bloch predictions for dE/dx of electrons and heavy particles show that the main background in this momentum

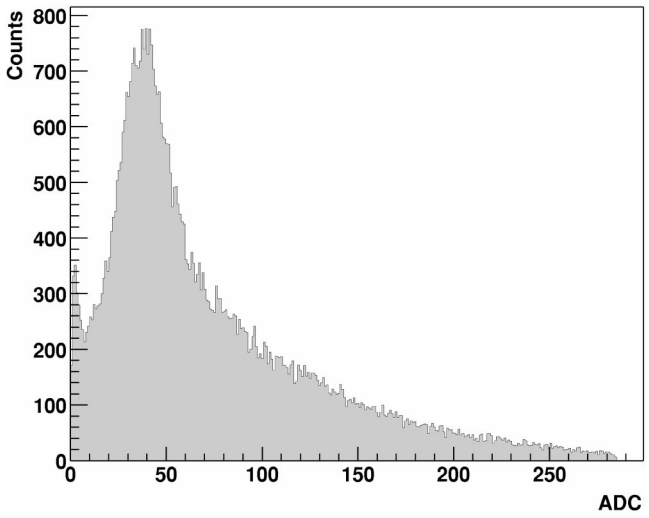

FIG. 1. Typical MIP spectrum. x-axis corresponds to ADC channel number. The hits correspond to isolated tracks with $p>1.25$ GeV/c which project to EMC towers. The peak corresponds to the energy deposited by nonshowering hadrons (MIP peak).

range comes from deuterons and heavier particles as well as the tails of the distributions of protons and lower mass particles. In order to minimize systematic uncertainties in this procedure, only tracks having a number of space points greater than 25 were used, as such "long tracks" exhibit better dE/dx resolution. It was also required that the track should be isolated in a 3×3 tower patch in the calorimeter.

As the final electron identifier, the energy, E_{tower}, deposited in the tower hit by the track is compared to the momentum, p, of the track in the range $1.5<p<5.0$ GeV/c. Figure 2 shows the p/E_{tower} spectrum for the electron candidates in which it is possible to see a well defined electron peak. The residual hadronic background in this figure can be evaluated by shifting the dE/dx selection window toward the pion region. The resulting estimate of the hadronic background is shown as a dashed line in the figure. After hadronic background subtraction, the peak position is still not centered at 1 due to the energy leakage to neighboring towers that is not taken into account in this procedure. The amount of leakage depends on the distance to the center of the tower hit by the electron and will shift the peak position to higher values as this distance increases. As shown in Fig. 3, this effect is reproduced well by the full GEANT simulations of the detector response when it is hit by electrons in the momentum range used in this calibration procedure. The upper plot of Fig. 3 shows the position of the electron p/E_{tower} peak as a

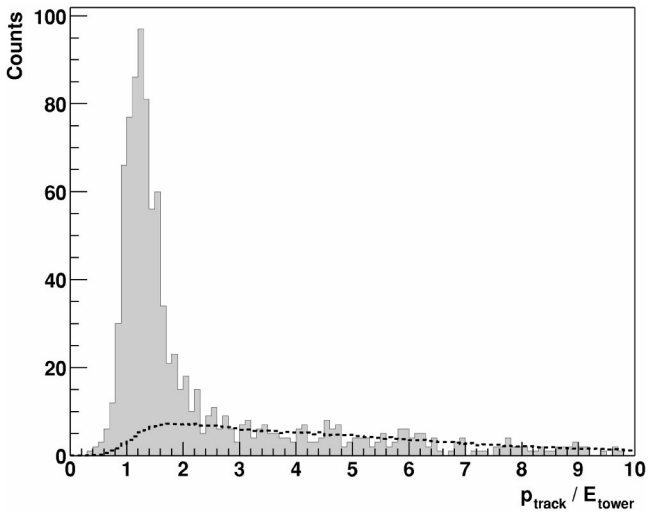

FIG. 2. p/E_{tower} spectrum for electron candidates, selected through dE/dx from the TPC, with $1.5<p<5.0$ GeV/c. A well defined electron peak is observed. The dashed line corresponds to the hadronic background in the dE/dx-identified electron sample.

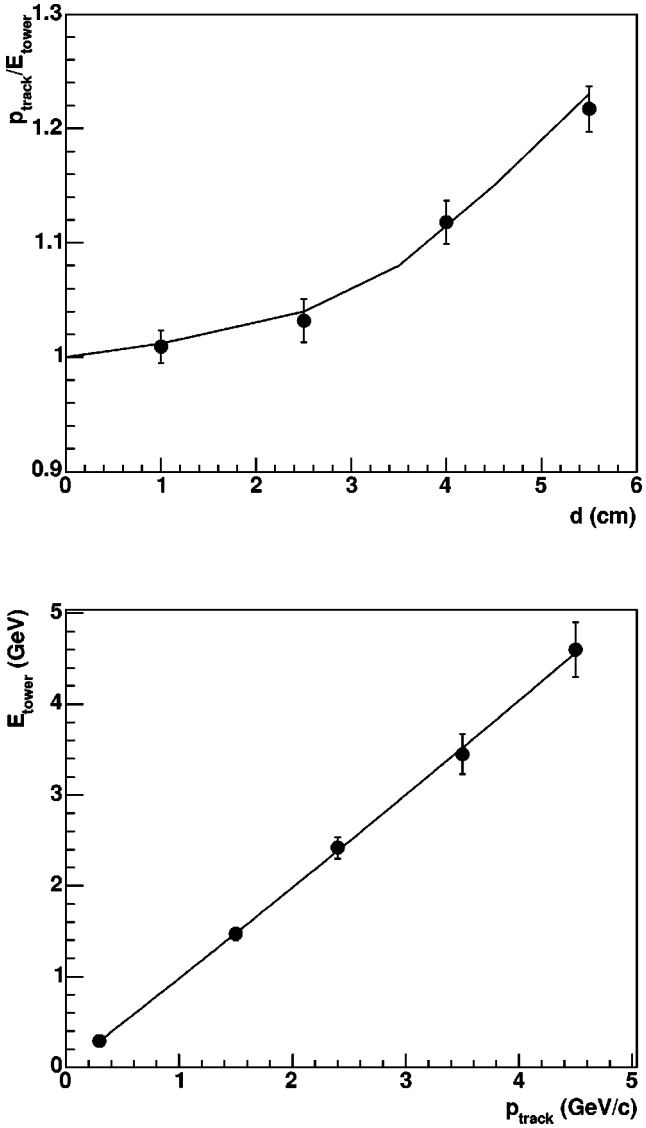

FIG. 3. Upper plot: points are measured p/E_{tower} electron peak position as a function of the distance to the center of the tower. The solid line is from a calculation based on a full GEANT simulation of the detector response to electrons. Lower plot: points show measured energy deposited by electrons in the tower as a function of the momentum for distances to the center of the tower smaller than 2.0 cm. The first point is the electron equivalent energy of the minimum ionizing particles. The solid line is a second order polynomial fit of the data.

function of this distance. The solid line is a prediction from GEANT simulations. The measurements are in good agreement with the simulations. Figure 3, lower plot, shows the energy deposited in the calorimeter tower as a function of its momentum for electrons in the case where the distance to the center of the tower is smaller than 2.0 cm. (A distance of 5 cm corresponds to the border of a tower at $\eta=0$. The border of the tower at $\eta=1$ is located 7.5 cm from its center.) The first point is the electron equivalent energy of the minimum ionizing particles. A fit to the data using the second-order polynomial of type $f(x)=a_0+a_1x+a_2x^2$ is represented by the solid line. The coefficients are $a_0=0.01\pm0.08$ GeV, $a_1=0.98\pm0.11$ c, and $a_2=0.01\pm0.03(\mathrm{GeV}/c^2)^{-1}$. The values of a_0 and a_2 are consistent with zero within errors. The small magnitude of these errors indicates that the detector response to electrons is very linear up to $p=5$ GeV/c.

By combining the MIP calibration and the electron calibration of the EMC, we obtain an overall estimated systematic uncertainty of less than 2% on the total energy measured by the calorimeter. The stability of the detector response was evaluated by monitoring the time dependence of the shape of the raw ADC spectra for each tower, which is the tower response for all particles that reach the calorimeter. In order to have enough statistics, each time interval is larger than one day of data taking but smaller than two days, depending on the beam intensity during that period. The overall gain variation of the detector was less than 5% for the entire RHIC run. The results reported in this paper were obtained from three consecutive days of data taking, in order to minimize any uncorrected effect due to gain variations in the detector.

B. Energy deposited by hadrons in the EMC

As discussed above, for the purposes of measuring electromagnetic energy production it is essential to subtract the hadronic energy deposition in the calorimeter. For charged hadrons, the hit locations on the calorimeter are well determined and if isolated, a cluster of energy is readily identified. In the dense environment of Au+Au collisions, however, it is difficult to uniquely identify the energy deposition associated with a specific hadron track. In this limit, which is relevant for the present measurement, we subtract an average energy deposition based on the measured momentum of the impinging track. Because we are interested in the cumulative distribution averaged over many events and because each event contains many tracks, this averaged correction results in a negligible contribution to the uncertainty in the measured electromagnetic energy.

We have studied hadron shower spatial and energy distributions in the calorimeter both experimentally, using well tracked and identified hadrons in sparse events in STAR, and in detailed GEANT simulations.

A library of separate profiles for pions, kaons, protons, and antiprotons was obtained from GEANT simulations of detector response in the STAR environment (GSTAR). The input events had a uniform momentum distribution in the range $0<p<10$ GeV/c and an emission vertex limited by $|z_{\mathrm{vertex}}|<20$ cm. The constraint on the longitudinal coordinate of the vertex insures that the trajectory of particles will extrapolate through only one tower of the EMC. Because the EMC is a projective detector, this constraint on the extrapolated track is strongly related to the vertex constraint. We projected the simulated tracks on the EMC using a helix model for the particle trajectory in a magnetic field and obtained the energy distributions and the corresponding mean values as a function of the momentum, the pseudorapidity of the EMC towers, and the distance of the incident hit point to the center of the tower (d). The distributions were binned in intervals of $\Delta\eta=0.2$. For all particles, the total mean deposited hadronic energy in a particular tower increases approximately linearly with the momentum, shows very little dependence on pseudorapidity, and decreases with increasing distance from the hit point to the center of the tower. Experimental hadronic shower profiles were obtained from Au+Au minimum bias data by projecting tracks on the EMC, accepting only those that were isolated in a 5×5 tower patch to ensure that the energy in the towers was from only one particle, and calculating the energy distributions and mean values. Profiles for all particles, except electrons and positrons, for both positive and negative tracks were recorded with good statistics up to momentum $p=2.0$ GeV/c.

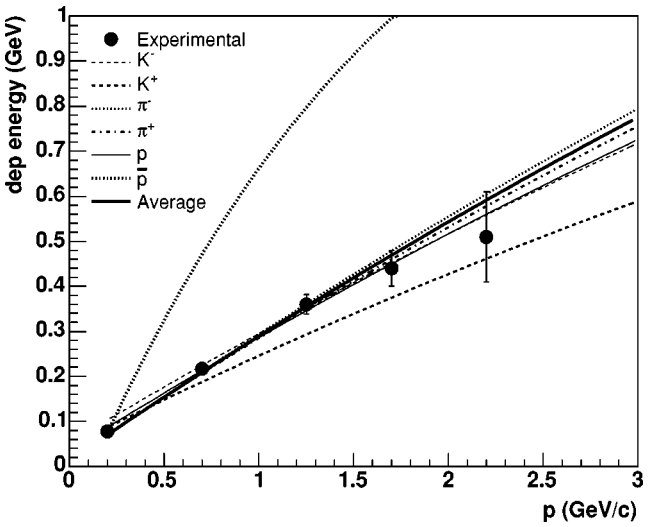

FIG. 4. Mean values from GEANT simulations of the energy deposited in the EMC by various hadronic species as a function of momentum.

In Fig. 4, we present the deposited energy for different particles from GEANT simulations as a function of momentum, for a fixed pseudorapidity and distance to the center of the tower. An average curve, based on the relative yield of the different particles, is also presented. Small differences are observed for most particles, except for the antiproton, for which the additional annihilation energy is apparent. The solid points are deposited energy obtained from experimental data for charged hadrons. The experimental profiles for charged hadrons agree quite well with the averaged profile. Because of the limited statistics, it was not possible to obtain the experimental profiles for identified hadrons. In Fig. 5, we present the simulated profiles for π^+ and π^- and the experimental profiles for all positively and negatively charged tracks in the momentum range $0.5<p<1.0$ GeV/c, as a

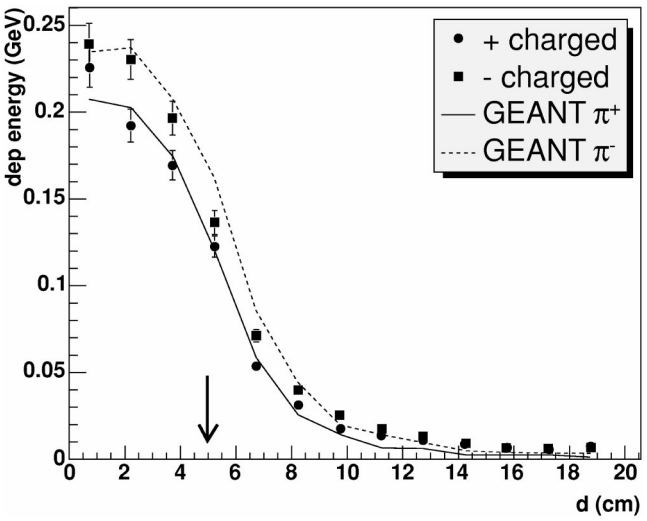

FIG. 5. Spatial profiles of energy deposition in the EMC as a function of distance (d) from the hit point to the center of the tower for π^+ and π^- from simulations and for positive and negative hadrons from data. The arrow indicates the distance corresponding to the border of a tower in $0<\eta<0.2$. An overall agreement between the shapes of the profiles is observed, with a small normalization difference (see text).

function of the distance to the center of a tower. The experimental profiles are well described by the simulation, except for a normalization factor on the order of 20% for $0<p<0.5$ GeV/c and 5% for $p>0.5$ GeV/c, as seen in Fig. 5. After renormalization, all experimental profiles up to momentum $p=2.0$ GeV/c are in good agreement with simulation and we therefore use the renormalized simulated profiles to allow smooth interpolation in the data analysis and for extrapolation to allow corrections for higher momentum tracks. However, since the interval $p<2.0$ GeV/c contains 98% of all tracks, the magnitude of this extrapolation is small for the E_T measurement.

C. E_T^{em} measurement

The electromagnetic transverse energy is defined as

$$E_T^{\mathrm{em}} = \sum_{\mathrm{towers}} E_{\mathrm{tower}}^{\mathrm{em}} \sin(\theta_{\mathrm{tower}}), \tag{5}$$

where $E_{\mathrm{tower}}^{\mathrm{em}}$ is the electromagnetic energy measured in an EMC tower and θ_{tower} is the polar angle of the center of the tower relative to the beam axis and the collision vertex position. Experimentally, E_T^{em} is given by

$$E_T^{\mathrm{em}} = \frac{1}{f_{\mathrm{acc}}} \sum_{\mathrm{towers}} (E_{\mathrm{tower}} - \Delta E_{\mathrm{tower}}^{\mathrm{had}}) \sin(\theta_{\mathrm{tower}}). \tag{6}$$

The sum over EMC towers corresponds to $0<\eta<1$ and $\Delta\phi=60°$. $f_{\mathrm{acc}}=\Delta\phi/2\pi$ is the correction for the acceptance, E_{tower} is the energy measured by an EMC tower, and $\Delta E_{\mathrm{tower}}^{\mathrm{had}}$ is the total correction for each tower to exclude the contribution from hadrons. The $\Delta E_{\mathrm{tower}}^{\mathrm{had}}$ correction is given by

$$\Delta E_{\mathrm{tower}}^{\mathrm{had}} = \frac{1}{f_{\mathrm{neutral}}} \sum_{\mathrm{tracks}} \frac{f_{\mathrm{elec}}(p_T)}{\mathrm{eff}(p_T)} \Delta E(p,\eta,d), \tag{7}$$

where $\Delta E(p,\eta,d)$ is the energy deposited by a track projected on an EMC tower as a function of its momentum p, pseudorapidity η, and distance d to the center of the tower from the track hit point. $f_{\mathrm{elec}}(p_T)$ is a correction to exclude electrons that are misidentified as hadrons and, therefore, should not be added to $\Delta E_{\mathrm{tower}}^{\mathrm{had}}$. This correction was estimated using the same procedure described in the previous section to exclude real electrons from the E_T^{had} measurement. $\mathrm{eff}(p_T)$ is the track efficiency, also discussed previously, and f_{neutral} is the correction to exclude the long-lived neutral hadron contribution. As in the case for E_T^{had}, $f_{\mathrm{neutral}} = \Delta E_{\mathrm{tower}}^{\mathrm{charged}} / (\Delta E_{\mathrm{tower}}^{\mathrm{charged}} + \Delta E_{\mathrm{tower}}^{\mathrm{neutral}})$ was estimated from the published STAR data at 130 GeV [28–31]. In this case, $\Delta E_{\mathrm{tower}}^{\mathrm{neutral}}$ is defined as the energy deposited by all long-lived neutral hadrons. The correction factor is $f_{\mathrm{neutral}}=0.86\pm0.03$.

The systematic uncertainty due to the track efficiency correction, as previously discussed, is 4%. The hadronic correction for charged tracks, $\Delta E(p,\eta,d)$, is based primarily on measured hadronic shower profiles with GEANT simulations used for interpolation between measurements and extrapolation beyond $p=2$ GeV/c. The systematic uncertainty for this correction to E_T^{em} is estimated from the observed uncertainties in the calculation of the hadronic profile at points in the shower library where full measurements were made. A 5% systematic uncertainty is consistent with the comparison of the measured and calculated shower profiles after normalization. Different from the hadronic component of transverse energy, there is no correction for p_T cutoff in the hadronic background subtraction in the electromagentic energy. Such low p_T tracks will not reach the calorimeter because of the strength of the magnetic field and, therefore, will not deposit energy in the detector.

As discussed earlier, the systematic uncertainty due to calibration of the detector is of the order of 2% and clearly this uncertainty contributes directly to the uncertainty in E_T^{em}. The systematic uncertainty due to the electron background track correction is negligible ($<0.5\%$).

The cumulative effect of all uncertainties discussed in this section, which are assumed to be uncorrelated, is an overall systematic uncertainty estimate for E_T^{em} of 8.0%. All corrections and the corresponding systematic uncertainties are summarized in Table II.

In order to evaluate the hadronic background subtraction procedure and estimate the event-by-event resolution of the reconstructed electromagnetic energy, we have performed simulations in which we compare the reconstructed E_T^{em} energy and the input from the event generator (HIJING). Figure 6 (upper panel) shows the ratio, event by event, of the reconstructed to the input electromagnetic transverse energy as a function of the raw energy measured by the calorimeter in the same acceptance used in this analysis. The smaller the raw EMC energy, the larger the impact parameter of the collision. The reconstructed energy, on average, is the same as the input from the event generator. Edge effects due to the limited acceptance of the detector were also studied and the

TABLE II. Corrections and systematic uncertainties for E_T^{em} for the 5% most central collisions. The quadrature sum of all systematic uncertainties, including the hadronic shower profiles subtraction $[\Delta E(p,\eta,d)]$ not shown in the table, results in a total systematic uncertainty of 8%. The upper part of the table shows the global correction and the bottom part shows track-wise corrections. In this case, the correction values for $p_T=0.25$ GeV/c and 1.0 GeV/c are shown.

Description	Correction
f_{neutral}	0.86 ± 0.03
$f_{\mathrm{elec}}(p_T)$	$0.96\pm<0.005$(0.25 GeV/c)
	$1.00\pm<0.005$(1 GeV/c)
$\mathrm{eff}(p_T)$	0.70 ± 0.04(0.25 GeV/c)
	0.80 ± 0.04(1 GeV/c)

effect on the reconstructed values, on average, is negligible. The event-by-event resolution, however, improves as the event becomes more central. Figure 6 (lower panel) shows the ratio distribution for the most central events. The solid line is a Gaussian fit, from which we estimate the event-by-event resolution of the reconstructed electromagnetic energy to be 14.5% for central events. The main factors that determine this resolution are the hadronic energy subtraction and the corrections for track efficiency and long-lived neutral hadrons. The effect on the global measurement due to the tower energy resolution, considering the EMC patch available, was estimated to be 0.5%, and that due to calibration fluctuations is 0.5%. The fluctuations due to the hadronic background subtraction procedure alone were estimated to be 12%, strongly dependent on the number of tracks used to correct the energy (for larger acceptances this resolution improves). The final E_T^{em} distribution is also corrected for vertex reconstruction efficiency.

V. TOTAL TRANSVERSE ENERGY E_T

The sum of E_T^{had} and E_T^{em} is the total transverse energy E_T of the events. In Fig. 7 we present the E_T distribution for minimum bias events, corrected for vertex reconstruction efficiency mainly in the low E_T region. The scale of the upper horizontal axis corresponds to the E_T measurement for the actual acceptance of $0<\eta<1$ and $\Delta\phi=60°$. The bottom axis is scaled to correspond to the E_T for full azimuthal coverage.

In Fig. 7 we also present the E_T distributions for different centrality bins defined by the percentages of the total cross section, selected on charged multiplicity with $|\eta|<0.5$. The centrality bin defined as 0–5 % (shaded area in Fig. 7) corresponds to the most central collisions amounting to 5% of the total cross section. The data for these centrality ranges are given in Table III. The centrality bins are determined by the uncorrected number of charged tracks with $|\eta|<0.5$ and the number of fit points larger than 10. The phase space overlap between the E_T and centrality measurements is small so that there is negligible correlation between them beyond that due to the collision geometry.

At the low energy edge, the distribution exhibits a peak, corresponding to the most peripheral collisions. For the largest values of E_T, the shape of the distribution is determined largely by statistical fluctuations and depends greatly on the experimental acceptance [35]. For larger acceptances, the decrease with increasing E_T is very sharp. For this measurement, the fall off of the distribution at large E_T is strongly dominated by the limited acceptance which, at this point, obscures any possible physics fluctuation. Combining the two contributions (hadronic and electromagnetic energies) to the total transverse energy and properly taking into account the correlated uncertainties, we estimate a combined systematic uncertainty in E_T of 7% and an event-by-event resolution of 17%. We obtained for the 5% most central collisions $\langle dE_T/d\eta|_{\eta=0.5}\rangle=\langle E_T\rangle_{5\%}=621\pm1(\mathrm{stat})\pm43(\mathrm{syst})$ GeV, scaled for full azimuthal acceptance and one unit of pseudorapidity.

The upper panel of Fig. 8 shows $\langle dE_T/d\eta\rangle$ per participant pair $N_{\mathrm{part}}/2$ as a function of N_{part} (obtained using Monte

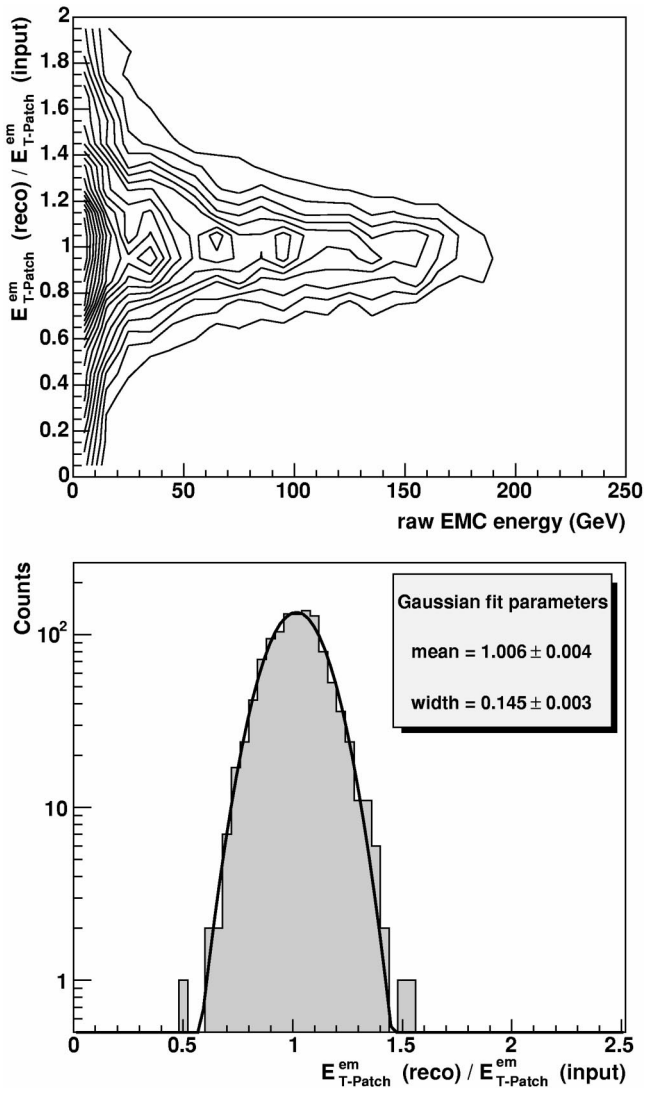

FIG. 6. Upper panel: Event-by-event ratio of the reconstructed electromagnetic energy and the input from the event generator as a function of the raw energy measured by the EMC. At 150 GeV, count numbers vary from 10 to 40 counts from the outer to the inner contour lines in steps of ~10 counts. Lower panel: The same ratio distribution for the most central events. The solid line is a Gaussian fit.

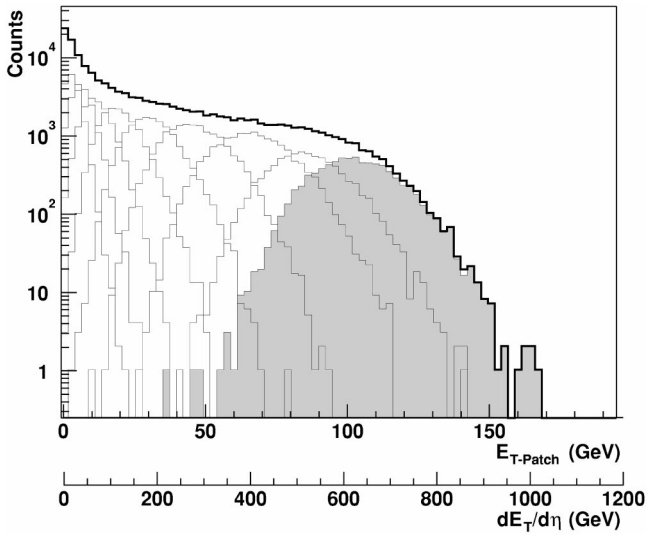

FIG. 7. Total transverse energy for $0<\eta<1$. The minimum bias distribution is presented as well as the distributions for the different centrality bins (see Table III). The shaded area corresponds to the 5% most central bin. The main axis scale corresponds to the E_T measured in the detector acceptance and the bottom axis is corrected to represent the extrapolation to full azimuthal acceptance.

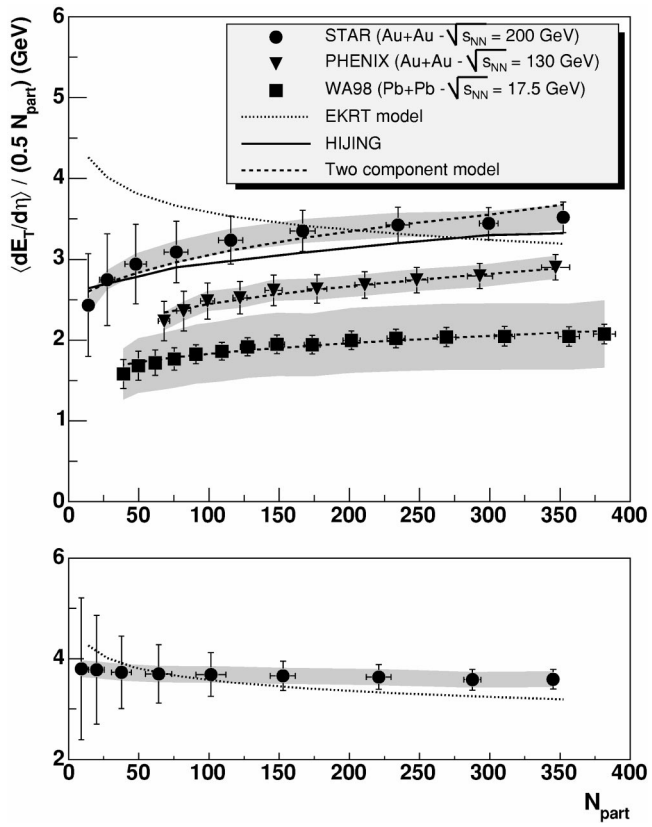

FIG. 8. $\langle dE_T/d\eta|_{\eta=0.5}\rangle$ per N_{part} pair vs N_{part}. Upper panel: N_{part} is obtained from Monte Carlo Glauber calculations. The lines show calculations using the HIJING model [27] (solid), the EKRT saturation model [7] [dotted, Eq. (8)], and the two-component fit (dashed, see text). Results from WA98 [14] and PHENIX [15] are also shown. The gray bands correspond to overall systematic uncertainties, independent of N_{part}. Error bars are the quadrature sum of the errors on the measurements and the uncertainties on N_{part} calculation. Lower panel: the same data are shown as in the upper panel but using and optical Glauber model calculation for N_{part}. The line shows the same result from EKRT model calculation.

Carlo Glauber calculations [20]). Data from Au+Au collisions at $\sqrt{s_{NN}}=200$ GeV from this analysis are shown together with similar measurements from Pb+Pb collisions at $\sqrt{s_{NN}}=17.2$ GeV from WA98 [14] and Au+Au collisions at 130 GeV from PHENIX [15]. These comparison measurements are at $\eta=0$, whereas the measurement reported here is at $0<\eta<1$. The gray bands for all three datasets show the overall systematic uncertainty of the data independent of N_{part}, while the error bars show the quadratic sum of the statistical errors, which are typically negligible, and the systematic uncertainties in E_T and N_{part} [20], with the latter dominating at low N_{part}.

A model based on final state gluon saturation (EKRT [7]) predicts a decrease in more central nuclear collisions for both the charged particle multiplicity per participant and E_T.

TABLE III. E_T and E_T^{em} as a function of the centrality of the collision. Global normalization uncertainties are indicated in the header of the table. All uncertainties are systematic. Statistical errors are negligible.

Centrality (%)	N_{part}	N_{bin}	E_T (GeV) ±4.3%	E_T^{em} (GeV) ±4.8%	E_T/N_{ch} (GeV) ±5.1%	$E_T/0.5N_{\text{part}}$ (GeV) ±4.3%	E_T^{em}/E_T ±3.4%
70 - 80	14±4	12±4	17.1±0.9	5.8±0.4	0.69±0.07	2.4±0.6	0.342±0.031
60 - 70	27±5	29±8	37.6±2.0	13.4±0.9	0.75±0.07	2.8±0.5	0.357±0.022
50 - 60	47±8	64±14	70±4	25.9±1.7	0.79±0.06	3.0±0.5	0.369±0.020
40 - 50	76±8	123±22	118±6	43±3	0.82±0.06	3.1±0.4	0.364±0.020
30 - 40	115±9	220±30	187±10	68±4	0.85±0.06	3.2±0.3	0.362±0.019
20 - 30	166±9	368±41	279±15	100±6	0.86±0.06	3.31±0.25	0.357±0.019
10 - 20	234±8	591±52	402±21	143±9	0.86±0.06	3.40±0.22	0.356±0.019
5 - 10	299±7	828±64	515±28	181±12	0.86±0.06	3.43±0.20	0.351±0.019
0 - 5	352±3	1051±72	620±33	216±14	0.86±0.06	3.51±0.19	0.348±0.019

TABLE IV. Two-component model fit results of $dE_T/d\eta = AN_{\rm part} + BN_{\rm bin}$. The uncertainties in the fit parameters include both the data and the $N_{\rm part}(N_{\rm bin})$ uncertainties.

	A (GeV)	B/A	$(B/A)(N_{\rm bin}/N_{\rm part})$
STAR	1.21±0.21	0.17±0.09	0.55±0.14
PHENIX	0.83±0.18	0.27±0.15	0.71±0.32
WA98	0.66±0.16	0.28±0.11	0.59±0.23

Hydrodynamic work during expansion may reduce the observed E_T relative to the initially generated E_T, perhaps by a factor ~3 at RHIC energies [7], though this effect will be offset somewhat by the buildup of transverse radial flow [7,8]. The dependence of observed E_T in $\sqrt{s}$ and system size A in the EKRT model is

$$E_T^{b=0} = 0.43A^{0.92}(\sqrt{s})^{0.40}(1 - 0.012 \ln A + 0.061 \ln \sqrt{s}). \quad (8)$$

The centrality dependence can be approximated by replacing A by $N_{\rm part}/2$ [36], shown by the dotted line in Fig. 8. The upper panel shows a comparison to measured $dE_T/d\eta$ per participant pair, incorporating a Monte Carlo Glauber calculation for $N_{\rm part}$. The EKRT model is seen not to agree with the data in this panel, missing significantly both the centrality dependence and the normalization for central collisions. A similar comparison is made in the lower panel of Fig. 8, which differs from the upper panel only in the use of an optical Glauber calculation for $N_{\rm part}$ [20]. The centrality dependence of the data in this case is reproduced well by the model, though ~15% disagreement in normalization for central collisions remains. More precise comparison of the system size dependence of E_T predicted by EKRT model to RHIC data requires either further refinement of the Glauber model calculations or measurements for central collisions with varying mass A.

The HIJING model predicts an increase in $\langle dE_T/d\eta\rangle/(0.5N_{\rm part})$, as shown in Fig. 8, upper panel. HIJING incorporates hard processes via the generation of multiple minijets together with soft production via string fragmentation. Effects of the nuclear geometry in HIJING are calculated using the Monte Carlo Glauber approach. Agreement of HIJING with the data is seen to be good in the upper panel.

We also study a simple two-component approach where $dE_T/d\eta = AN_{\rm part} + BN_{\rm bin}$. Using this model, it is possible to estimate the fraction of hard collisions in the E_T production. In this case, a simple fit function,

$$dE_T/d\eta/(0.5N_{\rm part}) = 2A[1 + (B/A)(N_{\rm bin}/N_{\rm part})], \quad (9)$$

is applied to our data at 200 GeV and the published PHENIX and WA98 results including points with number of participants larger than 100. The results from the fits are shown in Table IV. The simple scaling ansatz does a good job describing the overall shape of the $N_{\rm part}$ dependence at all energies. In this picture, the ratio $(B/A)(N_{\rm bin}/N_{\rm part})$ estimates the fraction of the transverse energy that scales like hard processes. As seen in the third column in Table IV, this ratio for the most central events is constant within errors despite the expectation that the cross section for hard processes grows by a large factor from 17 to 200 GeV.

We observe an overall increase in the transverse energy of (24±7)% at 200 GeV relative to 130 GeV. In Fig. 9, we present our result for dE_T/dy per participant pair for central collisions, together with results from other experiments at various collision energies from AGS to RHIC [12–15]. For the purposes of this comparison, we calculated dE_T/dy from $dE_T/d\eta$ for our measurements using a factor of 1.18 obtained from HIJING simulations to convert from η to y phase space. Our result is consistent with an overall logarithmic growth of $dE_T/dy/(0.5N_{\rm part})$ with $\sqrt{s_{NN}}$. The solid line is the prediction using the EKRT model [7] for central Au+Au collisions. As one can see, the EKRT model underestimates the final transverse energy by ~15%.

We have also estimated the spatial energy density produced in the collision using $\langle E_T\rangle_{5\%}$ reported above, converted from pseudorapidity to rapidity density using the factor of 1.18 discussed above. Based on a scaling solution to the relativistic hydrodynamic equations, Bjorken [16] estimated the spatial energy density of the system in terms of the primordial transverse energy rapidity density dE_T/dy, the transverse system size, R, and a formation time τ_0,

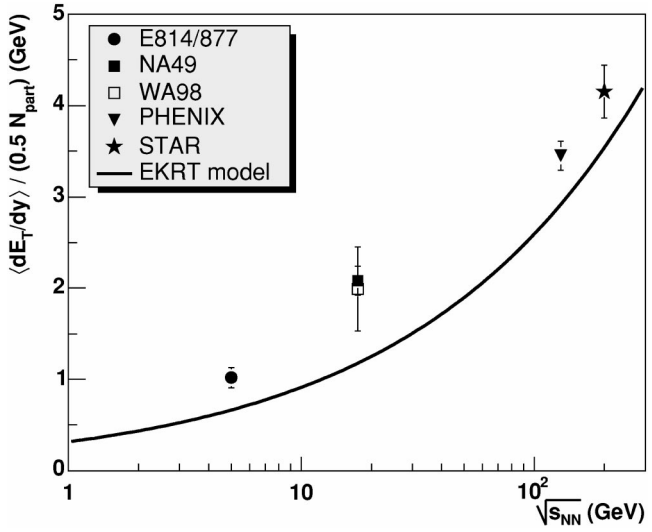

FIG. 9. dE_T/dy (see text for details) per $N_{\rm part}$ pair vs $\sqrt{s_{NN}}$ for central events. In this figure, $dE_T/dy/(0.5N_{\rm part})$ is seen to grow logarithmicaly with $\sqrt{s_{NN}}$. The error bar in the STAR point represents the total systematic uncertainty. The solid line is a EKRT model prediction [7], corrected for $d\eta/dy$, for central Au+Au collisions.

$$\varepsilon_{Bj} = \frac{dE_T}{dy}\frac{1}{\tau_0 \pi R^2}. \quad (10)$$

We assumed $\tau_0 = 1$ fm/c, which is the usual value taken in many analyses at SPS energies. For Au+Au at $\sqrt{s_{NN}} = 200$ GeV we obtained $\varepsilon_{Bj} = 4.9 \pm 0.3$ GeV/fm^3. The uncertainty includes only the uncertainty on $\langle dE_T/d\eta \rangle$. This energy density is significantly in excess of the energy density ~ 1 GeV/fm^3 predicted by lattice QCD for the transition to a deconfined quark gluon plasma [17]. The estimate is based, however, upon the assumption that local equilibrium has been achieved at $\tau \sim 1$ fm/c and that the system then expands hydrodynamically. Comparison of other RHIC data, in particular elliptic flow, to hydrodynamic calculations [37,38,39] indicates that this picture may indeed be valid.

In order to understand the systematic growth in transverse energy with collision energy shown in Fig. 9, we investigate the centrality dependence of $\langle dE_T/d\eta \rangle / \langle dN_{ch}/d\eta \rangle$, the scaling of transverse energy relative to the number of charged particles produced in the collision. The centrality dependence of this ratio may indicate effects of hydrodynamic flow [8]: if the expansion is isentropic, then $dN_{ch}/d\eta$ will remain constant, whereas $dE_T/d\eta$ will decrease due to the performance of longitudinal work.

Figure 10, upper panel, shows the centrality dependence of $\langle dE_T/d\eta \rangle / \langle dN_{ch}/d\eta \rangle$ from STAR measurements at $\sqrt{s_{NN}} = 200$ GeV, compared to similar measurements at 17 and 130 GeV. Data at all energies fall on a common curve within uncertainties, with modest increase from the most peripheral collisions to $N_{\text{part}} = 100$, reaching a roughly constant value of $\langle dE_T/d\eta \rangle / \langle dN_{ch}/d\eta \rangle$. Figure 10, lower panel, shows the $\langle p_T \rangle$ for 200 GeV Au+Au collisions measured by STAR [40], showing a dependence on centrality similar to that of the transverse energy per charged particle: modest increase with N_{part} for $N_{\text{part}} < 100$, with constant value for more central collisions. The systematic behavior of E_T, multiplicity, and $\langle p_T \rangle$ is similar, indicating that the growth of E_T is due to increased particle production. Quantitative comparison of theoretical models of particle production with the measured centrality dependences of $\langle dE_T/d\eta \rangle / \langle dN_{ch}/d\eta \rangle$ and $\langle p_T \rangle$ of charged particles will constrain the profile of initial energy deposition and the role of hydrodynamic work during the expansion.

In Fig. 11 we show, for central collisions, that this constant transverse energy production per charged particle is observed down to and including AGS measurements at $\sqrt{s_{NN}} = 5$ GeV. A single value of ~ 800 MeV per charged particle or at most a slow logarithmic increase amounting to $< 10\%$ characterizes all measurements within errors over a range in which the E_T per participant grows by a factor of 4. HIJING predicts that E_T per charged particle should increase from SPS to RHIC energies due to the enhancement of minijet production at RHIC. However, the predicted increase is rather small and the systematic uncertainties on the measurement do not provide enough precision to significantly test this assumption.

The procedures adopted in this analysis permit an independent measurement of the electromagnetic and hadronic transverse energy. This allows additional exploration of the collision dynamics and particle production. In Fig. 12 we show the ratio of the electromagentic to the total energy for the most central events as a function of the energy from lower SPS energies [11,41] to our results at full RHIC energy. The observed electromagnetic fraction of the total transverse energy will be strongly influenced by the baryon to meson ratio. At very high energy it is expected that virtually all the E_T will be carried by mesons and the fraction should approximate 1/3, whereas at low energy, baryon dominance of the transverse energy will result in a much smaller electromagnetic fraction.

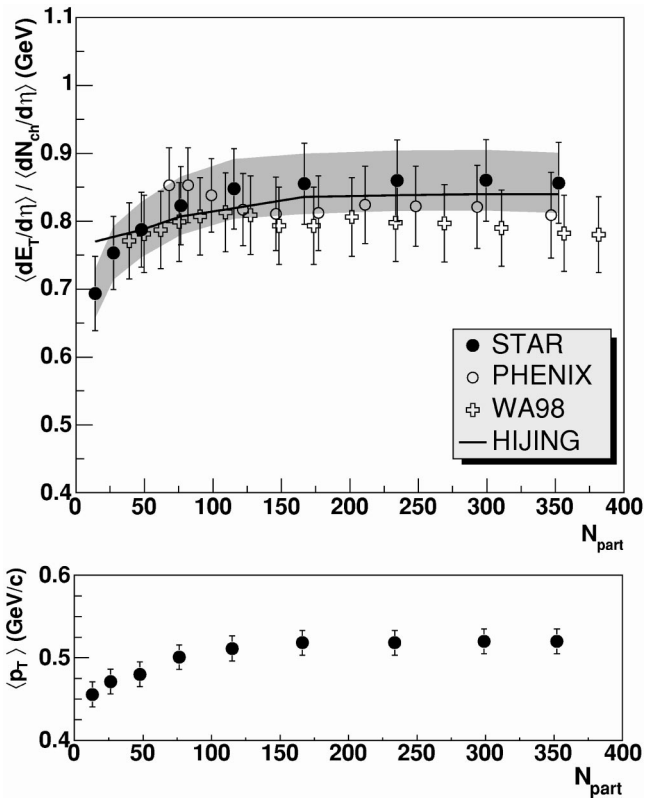

FIG. 10. Upper panel: $\langle dE_T/d\eta \rangle / \langle dN_{ch}/d\eta \rangle$ vs N_{part}. Predictions from HIJING simulations for Au+Au at 200 GeV are presented. Results from WA98 [14] and PHENIX [15] are also shown. The gray band corresponds to an overall normalization uncertainty for the STAR measurement. Bottom panel: Charged hadrons mean transverse momentum as a function of N_{part} [40].

While the energy dependence seen in Fig. 12 is presumably dominated by the total meson content of the final state, the centrality dependence may provide additional detail about the reaction mechanisms. The centrality dependence of the electromagnetic fraction of our total measured energy is shown in Fig. 13. An excess photon yield may result from the formation of a long-lived deconfined phase, as suggested in Ref. [42]. The predictions from HIJING simulations are also presented. We observe no significant dependence of the electromagnetic fraction with the collision centrality.

VI. SUMMARY

We have reported the measurement of transverse energy E_T within $0 < \eta < 1$, for centrality-selected Au+Au colli-

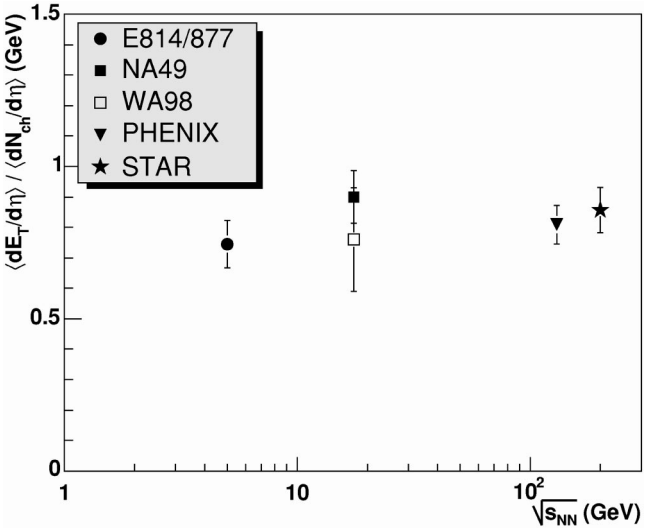

FIG. 11. $\langle dE_T/d\eta\rangle/\langle dN_{ch}/d\eta\rangle$ vs $\sqrt{s_{NN}}$ for central events. The error bar in the STAR point corresponds to the systematic uncertainty. A constant value of ~800 MeV per charged particle, within errors, characterizes transverse energy production over this full energy range.

sions at $\sqrt{s_{NN}}=200$ GeV. For the 5% most central events we measured $\langle E_T\rangle_{5\%}=621\pm1(\text{stat})\pm43(\text{syst})$ GeV, corresponding to an increase of $(24\pm7)\%$ with respect to measurements at 130 GeV Au+Au collisions at RHIC [15].

We investigated the energy scaling with the number of participant nucleons and with the number of charged particles produced in the collision. We obtained, for the 5% most central events, $dE_T/d\eta/(0.5N_{\text{part}})=3.51\pm0.24$ GeV and $\langle dE_T/d\eta\rangle/\langle dN_{ch}/d\eta\rangle=860\pm70$ MeV, respectively. We also compared the results of this work with measurements from AGS and SPS energies. It was found that the increase in the

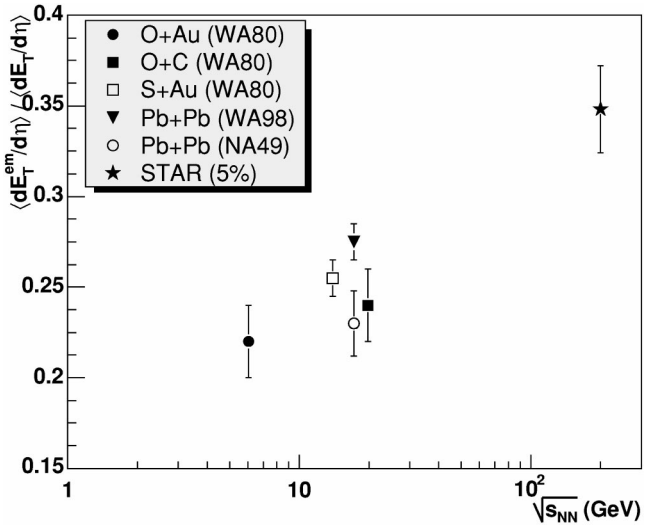

FIG. 12. Energy dependence of the electromagnetic fraction of the transverse energy for a number of systems spanning SPS to RHIC energy for central events.

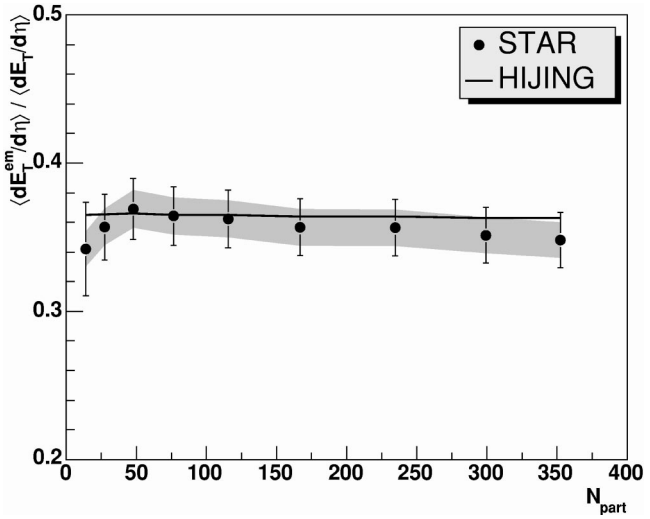

FIG. 13. Participant number dependence of the electromagnetic fraction of the total transverse energy. The results are consistent with HIJING within errors over the full centrality range.

E_T production from AGS up to RHIC energies comes mostly from the increase in the particle production. A final state gluon saturation model (EKRT), HIJING, and a simple two-component (hard/soft) model were compared to the data. Although the EKRT model predicts a different centrality behavior of energy production, the uncertainties in the N_{part} determination do not allow us to discard this model. The simple two-component ansatz suggests that, despite the large uncertainties, the fraction of energy arising from hard processes which is still visible in the final state does not increase significantly from SPS to RHIC energies.

Other measurements at RHIC and comparison to theoretical calculations suggest that a dense, equilibrated system has been generated in the collision and that it expands as an ideal hydrodynamic fluid. The good agreement between hydrodynamic calculations and measurements of particle-identified inclusive spectra and elliptic flow [38] is consistent with the onset of hydrodynamic evolution at a time $\tau_0<1$ fm/c after the collision [39]. The strong suppression phenomena observed for high p_T hadrons [43,44,45] suggest that the system early in its evolution is extremely dense. Estimates based on these measurements yield an initial energy density in the vicinity of 50–100 times cold nuclear matter density. Within the framework of boost-invariant scaling hydrodynamics [16], from the E_T measurement presented here we estimate an initial energy density of about 5 GeV/fm^3. This should be understood as a lower bound [6,9], due to the strong reduction in the observed relative to the initially produced E_T from longitudinal hydrodynamic work during the expansion. These three quite different approaches produce rough agreement for the estimated initial energy density, with a value well in excess of that predicted by lattice QCD for the deconfinement phase transition [17].

The method used in this analysis permitted an independent measurement of the electromagnetic and hadronic components of the total energy. The electromagnetic fraction of the transverse energy for the 5% most central events

obtained in this work is $\langle dE_T^{\mathrm{em}}/d\eta\rangle/\langle dE_T/d\eta\rangle = 0.35 \pm 0.02$, consistent with a final state dominated by mesons. Some models [42] expect that the formation of a long-lived deconfined phase in central events may increase the yield of direct photon production and, therefore, an increase in the electromagnetic fraction of the transverse energy. We, however, observe that the electromagnetic fraction of the transverse energy is constant, within errors, as a function of centrality. Measurements with larger acceptances would have systematic uncertainties significantly reduced and therefore would be able to show smaller effects that cannot be observed with the precision of the present measurement.

ACKNOWLEDGMENTS

We thank the RHIC Operations Group and RCF at BNL, and the NERSC Center at LBNL for their support. This work was supported in part by the HENP Divisions of the Office of Science of the U.S. DOE; the U.S. NSF; the BMBF of Germany; IN2P3, RA, RPL, and EMN of France; EPSRC of the United Kingdom; FAPESP of Brazil; the Russian Ministry of Science and Technology; the Ministry of Education and the NNSFC of China; Grant Agency of the Czech Republic, FOM and UU of the Netherlands, DAE, DST, and CSIR of the Government of India; Swiss NSF; and the Polish State Committee for Scientific Research.

[1] T. Roser, Nucl. Phys. **A698**, 23c (2002).
[2] J. P. Blaizot, Nucl. Phys. **A661**, 3c (1999).
[3] P. Jacobs and X. N. Wang, hep-ph/0450125.
[4] M. Jacob and P. V. Landshoff, Mod. Phys. Lett. A **1**, 657 (1986).
[5] X. N. Wang, Phys. Rep. **280**, 287 (1997).
[6] M. Gyulassy and T. Matsui, Phys. Rev. D **29**, 419 (1984).
[7] K. J. Eskola, K. Kajantie, P. V. Ruuskanen, and K. Tuominen, Nucl. Phys. **B570**, 379 (2000).
[8] P. F. Kolb, U. Heinz, P. Huovinen, K. J. Eskola, and K. Tuominen, Nucl. Phys. **A696**, 197 (2001).
[9] A. Dumitru and M. Gyulassy, Phys. Lett. B **494**, 215 (2000).
[10] G. R. Young, Annu. Rev. Nucl. Part. Sci. **42**, 237 (1992).
[11] WA80 Collaboration, R. Albrecht *et al.*, Phys. Rev. C **44**, 2736 (1991).
[12] J. Barrette *et al.*, Phys. Rev. Lett. **70**, 2996 (1993).
[13] T. Alber *et al.*, Phys. Rev. Lett. **75**, 3814 (1995).
[14] WA98 Collaboration, M. M. Aggarwal *et al.*, Eur. Phys. J. C **18**, 651 (2001).
[15] PHENIX Collaboration, K. Adcox *et al.*, Phys. Rev. Lett. **87**, 052301 (2001).
[16] J. D. Bjorken, Phys. Rev. D **27**, 140 (1983).
[17] F. Karsch, Nucl. Phys. **A698**, 199c (2002).
[18] S. Turbide, R. Rapp, and C. Gale, Phys. Rev. C **69**, 014903 (2004).
[19] WA98 Collaboration, M. M. Aggarwal *et al.*, nucl-ex/0006007.
[20] STAR Collaboration, J. Adams *et al.*, nucl-ex/0311017.
[21] STAR Collaboration, K. H. Ackermann *et al.*, Nucl. Instrum. Methods Phys. Res. A **499**, 624 (2003).
[22] M. Beddo *et al.*, Nucl. Instrum. Methods Phys. Res. A **499**, 725 (2003).
[23] M. Anderson *et al.*, Nucl. Instrum. Methods Phys. Res. A **499**, 659 (2003).
[24] C. Adler *et al.*, Nucl. Instrum. Methods Phys. Res. A **470**, 488 (2001).
[25] PHENIX Collaboration, S. S. Adler *et al.*, Phys. Rev. C **69**, 034909 (2004).
[26] P. Nevski, *Proceedings of the International Conference on Computing in High Energy and Nuclear Physics*, Padova, Italy (2000).
[27] X. N. Wang and M. Gyulassy, Phys. Rev. D **44**, 3501 (1991).
[28] STAR Collaboration, C. Adler *et al.*, Phys. Rev. Lett. **87**, 262302 (2001).
[29] STAR Collaboration, C. Adler *et al.*, Phys. Rev. Lett. **90**, 119903 (2003).
[30] STAR Collaboration, C. Adler *et al.*, Phys. Rev. Lett. **87**, 112303 (2001).
[31] STAR Collaboration, C. Adler *et al.*, nucl-ex/0206008.
[32] STAR Collaboration, C. Adler *et al.*, Phys. Rev. Lett. **89**, 092301 (2002).
[33] STAR Collaboration, J. Adams *et al.*, Phys. Rev. Lett. **92**, 112301 (2004).
[34] T. M. Cormier *et al.*, Nucl. Instrum. Methods Phys. Res. A **483**, 734 (2002).
[35] T. Abbott *et al.*, Phys. Rev. C **63**, 064602 (2001).
[36] D. Kharzeev and M. Nardi, Phys. Lett. B **507**, 121 (2001).
[37] T. S. Ullrich, Nucl. Phys. **A715**, 399c (2003).
[38] STAR Collaboration, J. Adams *et al.*, Phys. Rev. Lett. **92**, 052302 (2004).
[39] P. F. Kolb and U. Heinz, nucl-th/0305084 (2003).
[40] STAR Collaboration, J. Adams *et al.*, Phys. Rev. Lett. **91**, 172302 (2003).
[41] WA98 Collaboration, Systematic of Transverse Energy Production In ^{208}Pb Induced Collisions at 158 GeV/nucleon (1996).
[42] F. Halzen and H. C. Liu, Phys. Rev. D **25**, 1842 (1982).
[43] STAR Collaboration, C. Adler *et al.*, Phys. Rev. Lett. **89**, 202301 (2002).
[44] STAR Collaboration, J. Adams *et al.*, Phys. Rev. Lett. **91**, 072304 (2003).
[45] STAR Collaboration, C. Adler *et al.*, Phys. Rev. Lett. **90**, 082302 (2003).